Centrifuge modelling of rigid piles in soft clay

Klinkvort, R.T.; Poder, M.; Truong, P.; Zania, Varvara

Published in:
Proceedings of the 3rd European Conference on Physical Modelling in Geotechnics

Publication date:
2016

Document Version
Peer reviewed version

Centrifuge modelling of rigid piles in soft clay

R.T. Klinkvort
Klinkvort EURL, Montreuil, France

M. Poder
Rambøll, Copenhagen, Denmark

P. Truong
University of Western Australia, Perth, Australia

V. Zania
Technical University of Denmark, Lyngby, Denmark

ABSTRACT: Monopiles have so far been extensively used as foundation solutions for renewable energy, with the most popular being offshore wind developments. The current design practice of monopiles subjected to lateral loading has been widely questioned, because of the lack of empirical data. The objective of this study is to employ centrifuge modelling in order to derive experimental *p-y* curves for rigid piles embedded in over-consolidated soft clay. A kaolin clay sample was prepared and pre-consolidated by applying a constant pressure at the soil surface, while different over-consolidation ratios were achieved within the clay sample by carrying out the experiments at different g fields. The findings suggest that the normalised shape of the *p-y* curves can be predicted within a sufficient accuracy using the current methodology but that the ultimate lateral resistance is underestimated at shallow depths and overestimated at greater depths.

1 INTRODUCTION

Offshore wind farms have been shown as one of the most promising renewable energy sources. A majority of the offshore wind turbines installed today have monopile foundations and due to the existing technological know-how it may be the preferred foundation solution in the future deep water installations. According to the state of the practice the monopile foundation is designed using a Winkler approach, where the monopile is modelled as a beam and the soil as a set of uncoupled springs (*p-y* curves) (Reese & Van Impe, 2001). The accuracy of the current *p-y* formulation for monopiles has been widely discussed, even though it is recommended by the API (2011) and DNV (2014) design provisions. The *p-y* curve formulation for clay profiles is based on work performed for long flexible piles designed for Oil and Gas jackets (Matlock 1970). However monopiles behave as short rigid piles and several studies suggest that the ultimate resistance of piles in clay is underestimated by design provisions (Lau et al. 2014 and Zhang & Ahmari, 2011).

As shown in Figure 1 the two main parameters defining the *p-y* curve are: (a) the ultimate soil resistance p_u and (b) y_c which is defined as the displacement where half of the soil resistance is mobilized and is calculated as $y_c = 2.5\varepsilon_c D$ (D is the diameter of the pile and ε_c is the strain in an undrained compression test at half of the failure strength). The ultimate lateral resistance p_u in a cohesive soil can be found as:

$$p_u = N_p \cdot s_u \cdot D \tag{1}$$

where, s_u is the undrained shear strength and N_p is non dimensional earth pressure coefficient.

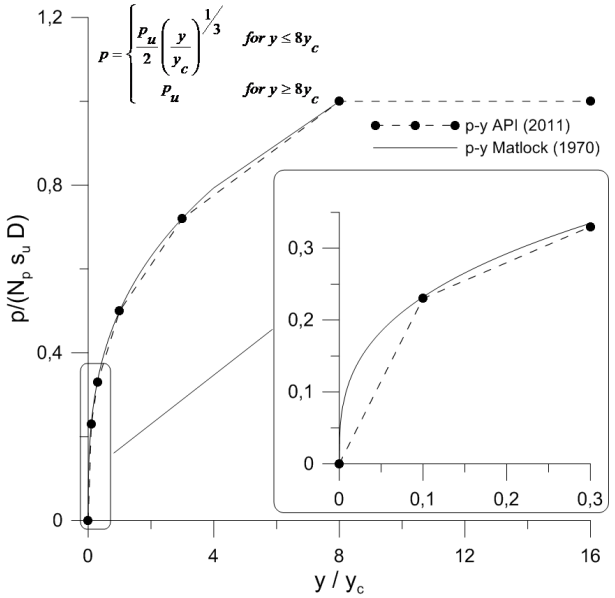

Figure 1. Normalized monotonic p-y curve for soft clay

The earth pressure coefficient N_p is defined by two different failure mechanisms, one deep failure mechanism where soil flows around the pile and one shallow failure mechanism where the soil is pushed upwards in a wedge. The earth pressure coefficient

can be found by plasticity theory and is 9 - 11 for the deep failure mechanism and decreasing to 3 at soil surface (Reese & Van Impe 2001). Both of these values are based on a smooth pile and a gap is developed behind the pile for the wedge type failure (Murff & Hamilton 1993). Even though offshore piles are regarded rough the offshore guidelines (API 2011) have adopted the values for smooth piles as given by:

$$N_p = \min\begin{cases} 3 + \dfrac{X \cdot \gamma'}{s_u} + J\dfrac{X}{D} \\ 9 \end{cases} \quad (2)$$

where X is the depth below soil surface, γ' is the effective unit weight of soil, and J is a dimensionless empirical constant ranging from 0.25 to 0.50. The shape of the *p-y* curves by Matlock (1970) and by API (2011) and DNV (2014) are shown in Figure 1, where the initial part of the curves is highlighted because it is particularly important for monopiles.

The current study aims at investigating the *p-y* response of rigid piles in soft clay, with a special focus of the initial stiffness and the ultimate lateral resistance. For this purpose centrifuge testing has been performed at two different g levels and the measured bending moment distributions have provided the basis of calculation of experimental *p-y* curves.

2 METHODOLOGY

The experiments were carried out in the geotechnical centrifuge at the Technical University of Denmark (Fuglsang & Nielsen 1988). The setup has been developed to test laterally loaded piles of large eccentricity (Klinkvort et al. 2013). A model monopile equipped with 15 half-bridge strain gauge levels was used to simulate the behaviour of a monopile and pre-consolidated Kaolin clay samples were considered to simulate soft clay.

2.1 *Preparation and consolidation of kaolin sample*

The Kaolin powder was mixed with water in the weight ratio of 1:1 to a homogenous consistency. This was followed by 4 hours of mixing under a vacuum of approximately 20 % of the atmospheric pressure. After mixing of the Kaolin slurry it was transferred to the strongbox for consolidation. A geotextile was placed in the circumference of the cylindrical container and a drainage layer at the bottom, facilitating faster drainage. The consolidation was performed by applying a constant pressure at a rigid lid placed at the soil surface. To avoid soil rupture the load was applied incrementally ensuring that each consolidation phase was finished, until the pressure reached the value of 250kPa. The monitoring of the consolidation was accomplished by measuring the displacement at the top of the lid. This procedure lasted 13 to 18 days for each one of the tests. When the consolidation phase was finalised the container was transferred and placed in the centrifuge.

Along with the centrifuge testing (Poder 2015) a series of classification and triaxial compression tests were performed at the Technical University of Denmark to determine engineering properties of the Kaolin (Mårbjerg 2015). The preparation technique was similar as in the centrifuge tests (mixing analogy the same but pre-consolidation of the slurry in the constant rate of strain, CRS) and one sample was taken directly from the centrifuge bucket. A summary of the test results is shown in Table 1.

Table 1. Summary of Kaolin properties

	Value
Specific gravity G_s	2.68
Earth pressure coefficient, K_o	0.68
Liquid limit, *LL*	56.1
Plasitic limit, *PL*	30.9
Plasticity index, PI	25.2
Water content (%)	49.0
Density, ρ	1.66
Critical sate parameters, *M*	1.10
Virgin slope, λ	0.174
Reload slope, κ	0.011
Shear strain at half failure strength, ε_{50} (%)	0.04-0.60

2.2 *Centrifuge test setup*

A sketch of the centrifuge setup for testing laterally loaded piles is shown in Figure 2. The embedment depth of the pile, (l_L= 6*D*) was selected to be representative of monopile foundations and the load eccentricity (l_e=9D) during the lateral loading, is achieved by applying displacement controlled load at the top hinge. Small variation in these lengths was seen between the tests mainly due to vertical pile movement. For this tests series the distance from the rotation point to the Kaolin surface was R_f=2.274m.

The model monopile used in the tests is a hollow steel pile with an outer diameter of 40 mm and an inner diameter of 35 mm. The pile thickness is 2.5 mm where 1 mm of this is an epoxy coating used to cover and protect the strain gauges. This gives a pile with a bending stiffness of EI=6.73kNm^2. The model pile is expected to behave as rigid, with Kr factors in the range of 0.7 to 7, since it is tested in a soft kaolin clay sample. 30 strain gauges are glued to the pile forming 15 half bridge strain gauge levels. All strain gauge bridges were calibrated prior to testing, to establish the bending moment from the gauge signals, showing linear responses. This allows to measure the moment in the pile during testing. An outer pipe to the barrel was connecting the bottom and top of the soil layer, ensuring a closed hydraulic connection.

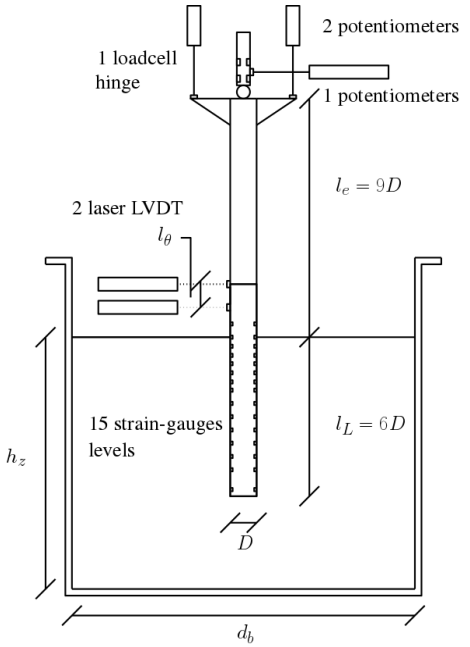

Figure 2. Schematic drawing of the centrifuge test setup.

All the tests were carried out with the same procedure, first the pile was jacked in the clay at the g-level which the lateral loading had been planned to be conducted. When the installation of the pile was completed the centrifuge was stopped and the setup was changed to enable lateral loading of the pile, similar to the approach described in (Klinkvort et al. 2013). Before the lateral loading of the monopile the centrifuge acceleration was kept constant for 30 minutes to ensure dissipation of excess pore water pressure generated due to the rotational acceleration and the increase in the g field. After this the lateral test was performed. Four tests were performed and named Test 2 to 5. Test 2 and 4 were carried out at an angular frequency of ϖ=12.56 (average acceleration 40g) and Test 3 and 5 at ϖ =16.75 (average acceleration 70g). The pile dimensions in prototype for the two g levels are: outer diameter 1.6m and 2.1m, thickness 60mm and 105mm, and length 9.6m and 19.8m respectively.

3 RESULTS

The interpretation of the lateral load tests requires establishing a strength profile within the sample. Hereafter the basis for calculation of the undrained shear strength within the clay sample is presented. The pre-consolidation and the given stress in the Kaolin sample leads to an over consolidation ratio (OCR). The over consolidation ratio (OCR) for the two acceleration levels is calculated as $OCR=\sigma'_{v,0}/\sigma'_v$ where $\sigma'_{v,0}$ is the vertical effective pre consolidation stress and σ'_v is the vertical effective stress in the centrifuge sample. The Kaolin sample is consolidated in the container by applying a vertical load on a top plate, hence friction develops along the geotextile attached to the side walls of the container and the consolidation stress will decrease with depth in the sample. The pre consolidation effective stress is therefore calculated as:

$$\sigma'_{v,0} = p - \Delta p \cdot z + z \cdot \rho' \cdot g \tag{3}$$

The vertical effective stress in the centrifuge sample increase with the rotation arm and is calculated as:

$$\sigma'_v = \rho' \cdot \varpi^2 \cdot z \cdot \left(R_t + \frac{z}{2} \right) \tag{4}$$

where z is the depth below soil surface, ρ' is the effective density of soil, R_t the distance from the center of rotation to the soil surface, and ϖ the angular frequency. The assumed pressure reduction Δp and applied pressure p are shown in Table 2. Under the final consolidation of Test 4 the loading system failed and the sample was standing in 4 days without any load before testing. This is considered as low apparent consolidation stress. The same decrease in consolidation stress due to side friction in the container was applied in all tests. The OCR is then decreasing with depth reaching a value of unity at the pile tip for the 4 tests.

Table 2. Parameters used to back-calculate pile installation to estimate the undrained strength.

	T2	T3	T4	T5
p (kPa)	250	250	90	250
Δ p (kPa/m)	35	35	35	35

The undrained shear strength in the soil sample is here estimated using the SHANSEP formulation (Ladd and Foote 1974):

$$\frac{s_u}{\sigma'_v} = \alpha \cdot OCR^{\beta} \tag{5}$$

Different values of α and β can be found in the literature, but here the values also used by Jeanjean (2009) for Kaolin are applied, where α and β were 0.19 and 0.67, respectively. The undrained shear strength here corresponds to the strength found in a constant volume Direct Simple Shear (DSS) test. The β value is the same whereas the α value is lower than seen in the triaxial compression tests (CIU). The reason for this is the different stress paths in the tests.

3.1 *Monotonic pile installation and estimation of undrained shear strength*

The strength distribution with depth will be further validated by assessing the installation force. The installation force of the monopiles, was recorded for all tests and can be seen in Figure 3. After each test the clay surface inside the pile was measured and it was between 1.0*D* and 1.5*D* lower than outside the pile. Hence the pile was plugged in the end of the installation for all the experiments. The estimate of the

undrained shear strength shown in Equation 5 is used together with the formulation for axial capacity of skirted foundations as proposed by Andersen et al. (2008) and shown in Equation 6 to back-calculate the installation force.

$$Q = \left(A_{out} + A_{in}\right) \cdot \alpha \cdot s_u^{DSS} + A_{tip}\left(N_c \cdot s_u^{AV} + \sigma'_v\right) \quad (6)$$

where, A_{out}, A_{in} is the area of outer and inner pile wall. A_{tip} is tip area, α is roughness factor, (taken as 0.45), s_u^{DSS}, s_u^{AV}: direct simple shear and average undrained shear strength. Here we assumed that $s_u = s_u^{DSS} = s_u^{AV}$. N_c is the end bearing capacity factor, equal to 9, σ'_v: effective overburden pressure at pile tip level.

The prediction of the pile installation force using Equations 5, and 6 is shown in Figure 3. There is a fairly good match between the penetration force for Test 2, and 4, whereas Tests 3 and 5 shows a good prediction of the installation force in the beginning until 4D of penetration and overestimates the penetration at the end of installation. The installation force for Test 5 is high, and a higher skin friction (α=0.6) was applied in order match the results. The discrepancy of the measured and predicted installation force close to the surface may be explained by the assumed constant reduction of the pressure due to side friction during consolidation. The OCR and the undrained strength are thus underestimated. A more elaborate procedure to estimate the OCR was not applied given the uncertainties to other parameters such as the roughness factor α.

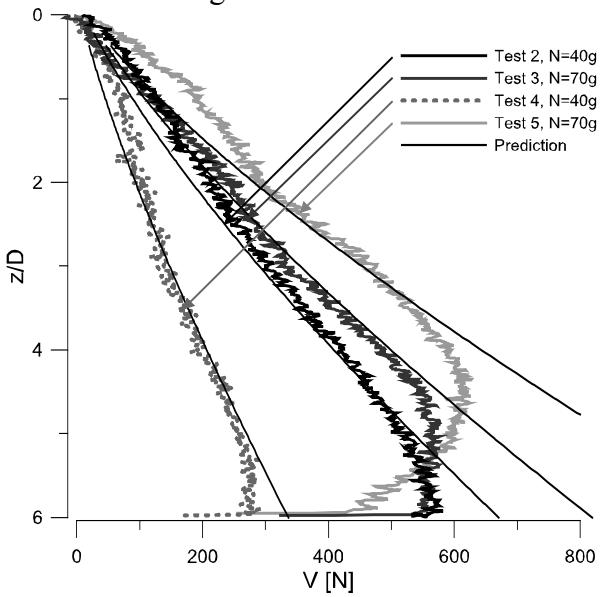

Figure 3. Monotonic pile installation force and pile installation prediction

3.2 *Monotonic lateral loading*

The total lateral response of the 4 tests is shown in Figure 4. Here the lateral load is normalised with the undrained average shear strength found at a depth of 2/3 of the pile length (l_L) and the diameter of the pile. The displacement at clay surface is normalised with the diameter. The normalised initial stiffness is identical for all tests. After a normalised load (H/s_uD^2) of 1, Test 4 shows remarkable different response compared to the rest of the tests. This together with the low installation strength makes the result from this test unreliable. Also the last part of Test 2 shows a response different from the other experiments. This should be kept in mind in interpretation of the soil pile interaction.

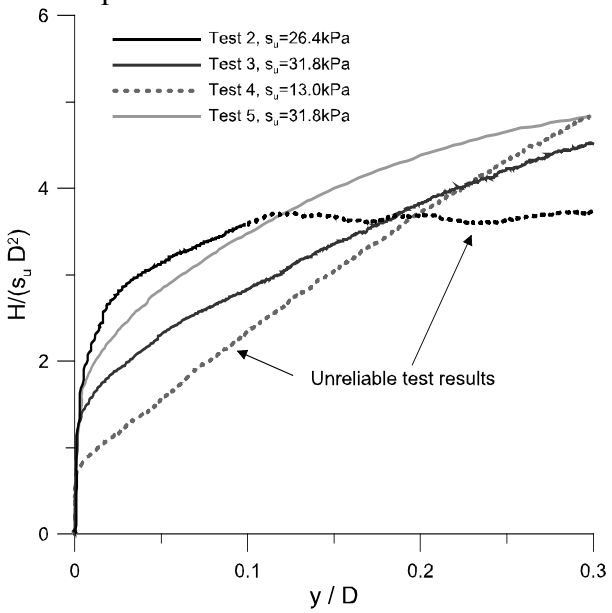

Figure 4. Load displacement response at the soil surface for the 4 tests. s_u is found in a $z = 2/3l_L$.

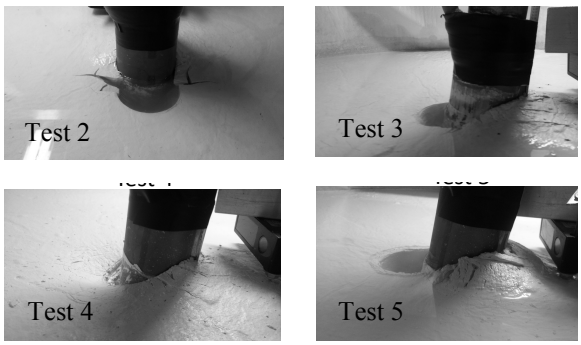

Figure 5. Failure mode after lateral loading for the 4 tests.

Figure 5 presents the observed failure of the clay after the lateral load test. In all tests except test 4 there is a clear gap formed at the rear side of the pile, while the clay is bulging in the front side of the pile for all tests. This could explain the different behaviour in the load displacement response of Test 4. Regarding Test 2, the perpendicular cracks in the clay in the rear side of the pile, might have induced the softening response at the load displacement curve.

3.3 *Pile soil interaction (p-y curves)*

The moment at each strain gauge level was logged during lateral loading. For each load step the moment distribution in the pile has been fitted with a 7th order polynomial. Using beam theory the soil resistance (p) can be found by a double differentiation

of the polynomial fit of the moment distribution. In a similar way the displacement (y) is found by a double integration of the polynomial fit of the moment. Other fitting methods (piecewise polynomial and finite difference) have been also implemented and the established p y curves were consistent. Figure 6 shows a typical result of the soil pile interaction curves from the centrifuge tests, with Test 5 presented as an example. The global response the local curves also shows the same initial stiffness. The capacity of the curves are clearly a function of depth and all curves until a depth of 3.5D show a clear maximum capacity. The point of rotation is in-between 4.0D and 4.5D hence the curve from a depth of z=4.0D is close to the point of rotation and the maximum soil resistance is not mobilised due to small displacements.

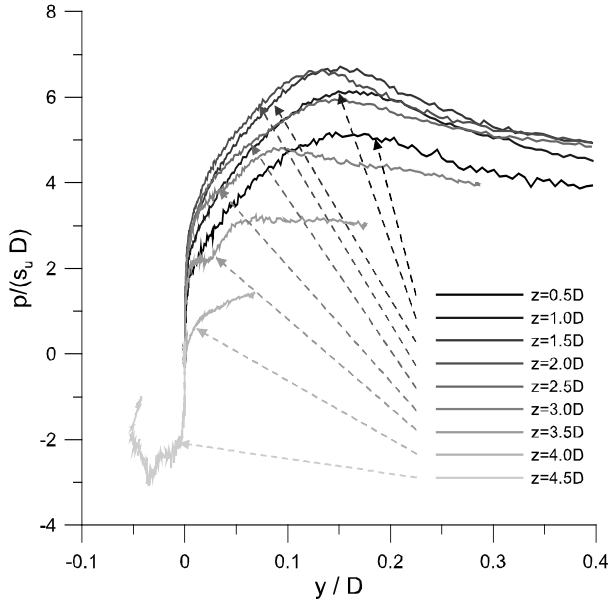

Figure 6. Typical p-y curves for the centrifuge tests, Test 5

4 DISCUSSION

Pile soil interaction curves have been generated for all tests and have showed local responses similar to the ones in Figure 6. The assumptions made in order to analyse the data further and to compare with design guidelines are discussed in this section along with the application for new design.

4.1 *Undrained strength profile*

The undrained strength profile was based on a back-calculation of the pile installation and is therefore subjected to some uncertainties. A relative good fit was achieved for two of the tests but some difference was observed in the measured and predicted pile installation force. Also the plugging that was observed in the test was not predicted. The triaxial tests confirmed the range of undrained shear strength values and provide an estimate of the stiffness and strength of the tested Kaolin.

4.2 *Pile soil interaction (p-y curves)*

The pile soil interaction curves that have reached an ultimate value from Test 2 – 3 – 5 are plotted in Figure 7. The curves have here been normalised with capacity ($N_p\ s_u\ D$) and displacement where the capacity is reached (δy_c). This allows the comparison with models proposed by Matlock (1970) and Jeanjean (2009). Table 3 shows the displacement parameters needed for the different tests. The values are not identical but within the same range. The curves from the tests show a similar behaviour for all tests. Even though there is some scatter in the results in the initial part it can be seen that the original shape proposed by Matlock (1970) and the shape proposed by Jeanjean (2009) seems to capture the initial stiffness best.

Table 3. Strain at half mobilisation and normalised deflection at maximum soil resistance

	T2	T3	T4	T5
ε_c (%)	0.4	1.0	2	0.6
y_c (D)	0.08	0.2	0,4	0.12

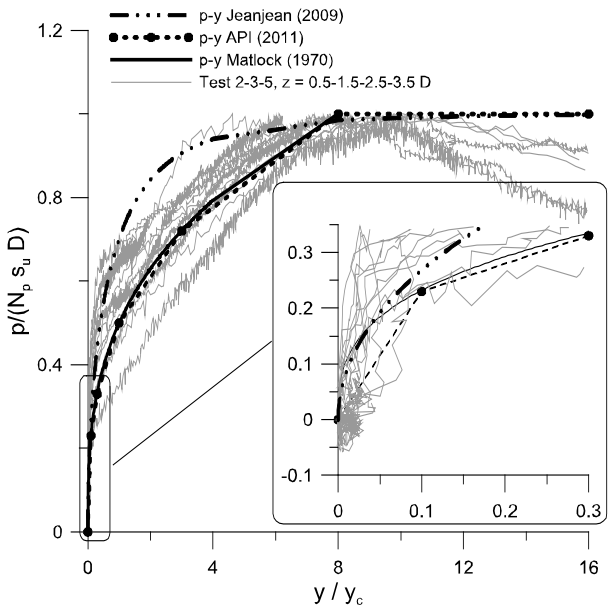

Figure 7. Normalised p-y curves from Test 2-3-5.

After approximately a mobilisation of 40% of the normalized ultimate resistance the shapes proposed by Matlock (1970) and Jeanjean (2009) starts to deviate and the results from the tests plots in between the recommendations. Overall the two recommendations provide an upper and a lower bound to the experimental results. One general difference from the two models and the test results is the softening centrifuge test curves. At the point of softening the pile has been displaced more than 0.4 – 1.0 D and the softening may be a consequence of the boundary condition at pile head. The pile head was not allowed to move in a vertical direction during tests 4 and 5. This result in a reduction of the axial force during loading and the pile tend to be lifted at large

displacement. The softening part of the curves reported here is therefore uncertain.

4.3 *Capacity*

The bearing capacity coefficient used to normalise the results in Figure 6 is here plotted and compared in Figure 7. The bearing capacity coefficient obtained from the experimental *p–y* curves suggests that the lateral bearing capacity factor N_p is underestimated at shallow depths and overestimated at greater depths by design provisions API (2011). It also shows that values found in the centrifuge and numerical analysis by Jeanjean (2009) here overestimates the value in all depths. The reason for the overestimation by Jeanjean (2009) is the assumption of double wedge failure. In the centrifuge tests, presented here, a crack was clearly seen behind the pile. For monopiles supporting offshore wind turbines the load is applied with few seconds, this is in contrast to the centrifuge test here where the load is applied slowly. The effect of load rate can therefore be very important for the capacity of the monopiles. This needs to be addressed in future study.

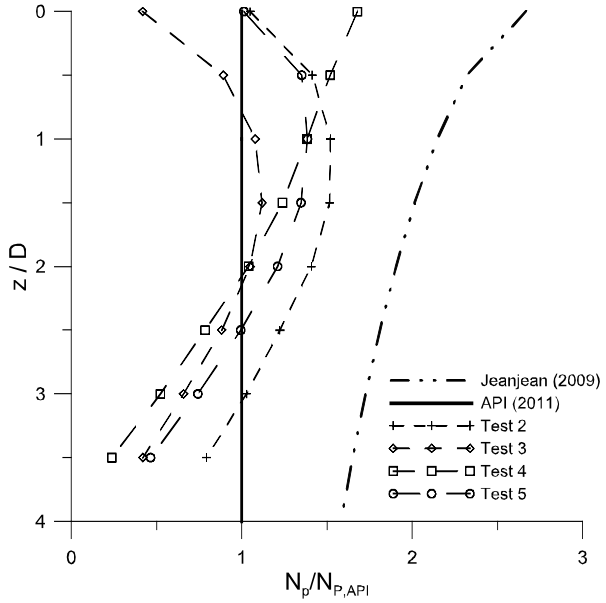

Figure 8. Comparison of bearing capacity factor found from the tests with the prediction by API (2011), using J=0.5. The prediction by Jeanjean (2009) using λ=0.25 is also shown.

In both Matlock (1970) and Jeanjean (2009) approaches the normalised bearing capacity factor is assumed to increase to a given depth and is thereafter constant. The assumption is flow around mechanism where soil is moving around the pile in a horizontal plane. These centrifuge tests suggest that this is not the case for short rigid piles. The failure mode for these pile are different from the slender piles. It can be seen from the centrifuge tests that the factor is decreasing when it approaches the rotation depth. This suggests some interaction with the rotation mode.

5 CONCLUSION

This paper presents the results of four centrifuge test in soft clay. The ultimate lateral resistance obtained suggests that the lateral bearing capacity factor N_p proposed by design guidelines is slightly underestimated at shallow depths and overestimated at greater depths. The initial stiffness of the *p-y* curves seem to be underestimated slightly but the general shape is described with a reasonable accuracy. To update the current design guidelines more special designed tests are needed with a big focus on load conditions similar to offshore wind turbines and to obtained engineering parameters of the soil samples.

REFERENCES

API 2011. *ANSI/API recommended practice 2GEO first edition, Petroleum and natural gas industries: Specific requirements for offshore structures. Part 4. Geotechnical and foundation design considerations.* API.

Andersen, K.H. Jostad, H.P. & Dyvik, R. 2008. Penetration Resistance of Offshore Skirted Foundations and Anchors in Dense Sand, *Journal of Geotechnical and Geoenvironmental Engineering*, 134(1): 106-116.

DNV 2014. *Offshore standard dnv-os-j101, Design of offshore wind turbine structures*. Offshore Standard DNV-OS-J101.

Fuglsang, L.D. & Nielsen, J. 1988, Danish centrifuge hardware and usage, *Centrifuges in Soil Mechanics*, 93-95.

Jeanjean P. 2009. Re-Assessment of p-y Curves for Soft Clays from Centrifuge Testing and Finite Element Modelling. *OTC-20158-MS. Offshore Technology Conference, 4-7 May, Houston, Texas.*

Klinkvort, R.T., Hededal, O. & Springman, S.M. 2013. Scaling issues in centrifuge modelling of monopiles. *International Journal of Physical Modelling in Geotechnics* 13(2): 38-49

Ladd, C.C., & Foote, R. 1974. A new design procedure for stability of soft clays. *Journal of the Geotechnical Engineering Division*. *ASCE*, 100 (7): 763-786.

Lau, B.H., Lam, S.Y., Haigh, S.K., & Madabhushi S.P.G 2014. Centrifuge testing of monopile in clay under monotonic loads. In Gaudin & White (Eds) *Physical modelling in geotechnics*, London: Taylor & Francis group.

Matlock 1970. Correlation for design of laterally loaded piles in soft clay. *OTC-1204-MS. Offshore Technology Conference, 22-24 April, Houston, Texas*

Murff, J.D. & Hamilton, J.M. 1993 P-ultimate for undrained analysis of laterally loaded piles. *Journal of Geotechnical Engineering*.119(1):91-107.

Mårbjerg, M.K. 2015. *Numerical modelling of lateral loaded piles in clay.* Master Thesis. Technical University of Denmark

Poder, M. 2015 *Experimental investigation of the bearing capacity of monopile foundation*. Master Thesis. Technical University of Denmark.

Reese, L. C. & Impe, W. F. V. (2001). *Single Piles and Pile Groups Under Lateral Loading*, CRC Press, Taylor & Francis Group.

Zhang, L. & Ahmari, S. 2011. Nonlinear analysis of laterally loaded rigid piles in cohesive soil, *International Journal for Numerical and Analytical Methods in Geomechanics*, 37(2):201-220..